AC Conductivity and Dielectrical Properties of Bulk $TlInSe_2$

M.H. Ali*

Physics Department, Faculty of Science, Ain Shams University, Abbassia, 11556 Cairo, Egypt.
*E-mail: mhali_55@hotmail.com

AC conductivity and dielectric properties of bulk $TlInSe_2$ were studied in the frequency and temperature range of 42-1 MHz and 294-473 K, respectively. The XRD pattern showed that the powder of $TlInSe_2$ has a tetragonal structure. AC conductivity, σ_{ac} (ω), as a function of frequency varies as power law: σ_{ac} (ω) = B ω^s. Temperature dependence of frequency exponent was analyzed to predict the conduction mechanism, which was found to be correlated barrier hoping model (CBH). Frequency and temperature dependences of dielectric constant and dielectric loss were also investigated. Electric modulus formalism was applied for evaluating the activation energy of the dielectric relaxation process.

1. Introduction

$TlInSe_2$ crystals belong to the III-III-VI_2 family known as thallium dichalcogenides. Members of this family have both layered ($TlGaS_2$, $TlGaSe_2$ and $TlInS_2$) and chain ($TlInSe_2$, $TlInTe_2$ and $TlGaTe_2$) structures [1,2]. Members of this family have anisotropic crystal structure and reported to have promising properties and technological applications. Several reports on x-ray detector [3], effective switching and memory elements [4], promising thermoelectric materials [5,6] and as superionic conductivity [7].

Due to the interesting properties, the low dimensional TlSe and $TlInSe_2$ single crystals have attracted the attention of researchers [5,8-13]. $TlInSe_2$ crystal is reported to have different applications. Tl-$TlInSe_2$ heterojunction sensitive to light and hard radiation was reported [8]. Semiconductor detector of neutron radiation, based on $TlInSe_2$ crystal, has been investigated [9]. The detector has high sensitivity and small size. It is capable of monitoring spatial, time and intensity distribution of γ rays and neutrons. In addition, $TlInSe_2$ crystal has been used as semiconductor filter to the polymer composites on the basis of polyethylene and polypropylene [10]. Therefore, there are extensive studies on

$TlInSe_2$ single crystals, in view of possible application in optoelectronics due to their high photosensitivity in the visible spectral range, high birefringence and broad transparency range [11]. Moreover, photoinduced phenomena enabling memory effects [12] and its high Seebeck coefficient make $TlInSe_2$ promising material for thermoelectric devices [13].

Some physical properties of $TlInSe_2$ crystal have been studied. Reports on: electrical conductivity [14], optical properties [15], photoconductivity [16], Raman scattering [17,18] and thermoelectric power [13]. There was no detailed study for ac conductivity measurements. Therefore, this work aim is to study and analyze the ac conductivity and dielectrical properties of bulk $TlInSe_2$ as a function of frequency and temperature.

2. Experimental Technique

$TlInSe_2$ was prepared by weighed the appropriate amounts of high purity elements of Se, In and Tl (5N) and then were sealed in evacuated quartz ampoule. This ampoule was heated to 1200 K for 10 h. The molten sample was then allowed to cool to room temperature at a rate of 10 K/hour. The composition and homogeneity of the $TlInSe_2$ powder were checked by energy dispersive X-ray spectroscopy (EDX) attached to scanning electron microscope (JEOL 5400). The X-ray diffraction (XRD) study was performed using Philips X´pert diffractometer with CuK_α radiation. $TlInSe_2$ ingot was well ground to obtain fine powder form. The powder is pressed in the form of pellet of diameter 0.9 cm and thickness 500 μm. The two opposite faces of the pellet were coated with Au thin film to serve as ohmic electrodes. Au thin films were evaporated using Edward 306A thermal evaporation unit under vacuum of $\sim 1.33\times 10^{-4}$ Pa. The dielectric measurements were carried out using programmable RLC bridge, model Hioki 3532-50 LCR HiTester, in the frequency range of 42 Hz to 1MHz and in temperature range 293-473 K. The impedance, Z, the capacitance, C, and the loss tangent, tan δ, of the samples were measured. The temperature was measured using Chromel-Alumel thermocouple. The accuracy in the measurement of dielectric constant is ~ 0.001 and that of loss is $\sim 10^{-4}$.

3. Results and Discussion

The X-ray diffraction pattern of the $TlInSe_2$ powder is shown in Fig. (1). The diffraction pattern confirms the crystalline nature of $TlInSe_2$. The indexing of the diffraction pattern reveals that there is good agreement with the reported data [19]. $TlInSe_2$ is tetragonal crystal structure with lattice parameters of a=8.075 Å and c= 6.847 Å [19].

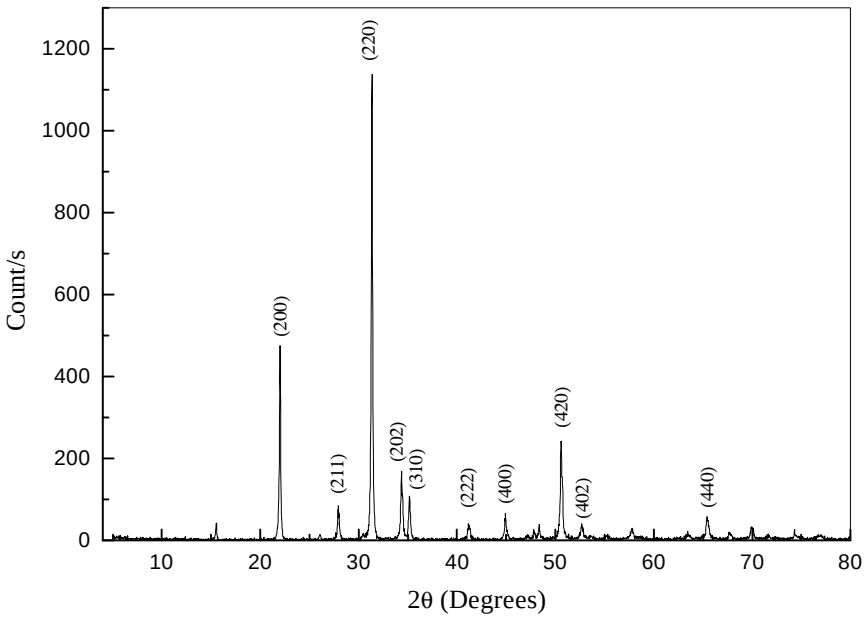

Fig. (1): XRD pattern of the powder of $TlInSe_2$.

3.1. Frequency and Temperature dependences of σ_{ac} (ω)

The common feature of semiconductors that the total conductivity is a sum of the two components: dc conductivity (σ_{dc}), which is independent of frequency; and frequency dependent conductivity (σ_{ac}) [20,21] :

$$\sigma_t(\omega) = \sigma_{dc}(0) + \sigma_{ac}(\omega) \quad (1)$$

The total conductivity $\sigma_t(\omega)$ was calculated from the well-known relation: $\sigma_t(\omega) = \frac{d}{ZA}$, where ω is the angular frequency, d is the sample thickness, Z is the sample impedance and A is the cross-sectional area. The values of σ_{dc} were obtained by extrapolating $\sigma_t(\omega)$ to ω=0. Thus, the ac conductivity $\sigma_{ac}(\omega)$ of $TlInSe_2$ was calculated using Eq.1. Figure 2 shows the frequency dependence of the ac conductivity, $\sigma_{ac}(\omega)$ of $TlInSe_2$ at various constant temperatures. It can be observed that $\sigma_{ac}(\omega)$ increases with increasing frequency and increases with increasing temperatures in the investigated range. The behavior of ac conductivity with frequency obeys the following formula [22,23]:

$$\sigma_{ac}(\omega) = B\,\omega^S \quad (2)$$

where B is a constant dependent on temperature and s is the frequency exponent [24]. The frequency exponent s was determined from the slope of the straight lines of *log* σ_{ac} – *log* ω plots (Fig. 2) at different constant temperatures. It was found that the values of frequency exponent decrease with increasing temperature as seen in Fig. 3. Various models have been proposed to explain the behavior of the frequency exponent s, for semiconducting glasses [25-29] as Quantum–mechanical tunneling (QMT), small polaron tunneling (SPT), large polaron tunneling (LPT) and correlated barrier hopping (CBH) models [21]. Our results suggest that the correlated barrier hopping model is the most suitable model to characterize the ac electrical conduction mechanism of $TlInSe_2$. This model predicts a temperature-dependent of s, which decreases with increasing temperature. In CBH model, the charge carriers are assumed to hop over the potential barrier separating neighboring localized sites. The frequency exponent s for hopping model is given by [30]:

$$s = 1 - \left(\frac{6\,kT}{W_M}\right) \tag{3}$$

where W_M is the maximum barrier height, k is Boltzmann constant and *T* is the absolute temperature. The value of W_M was determined to be 1.39 eV from the slope of the obtained straight line for the dependence between 1-s and temperature as shown in Fig. (4) using Eq. (3).

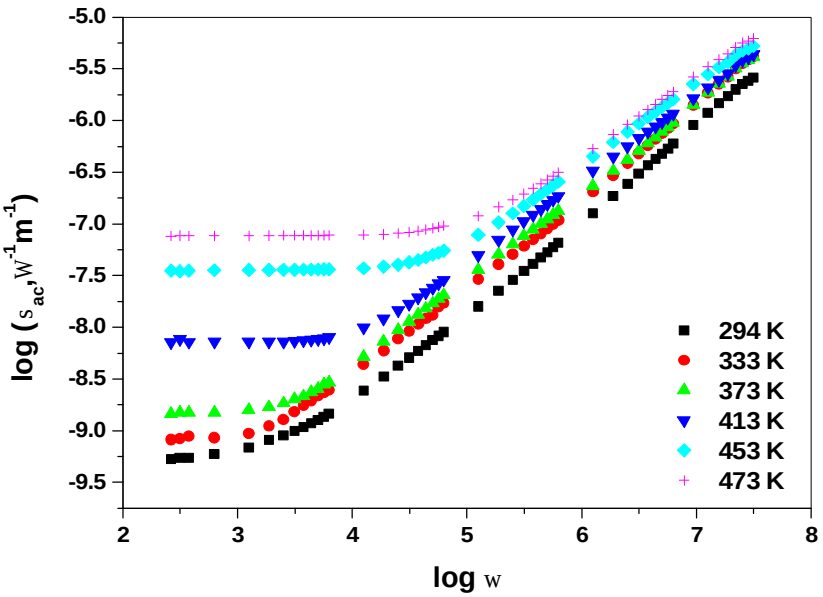

Fig. (2): Frequency dependence of σ_{ac} for $TlInSe_2$ at different Temperatures.

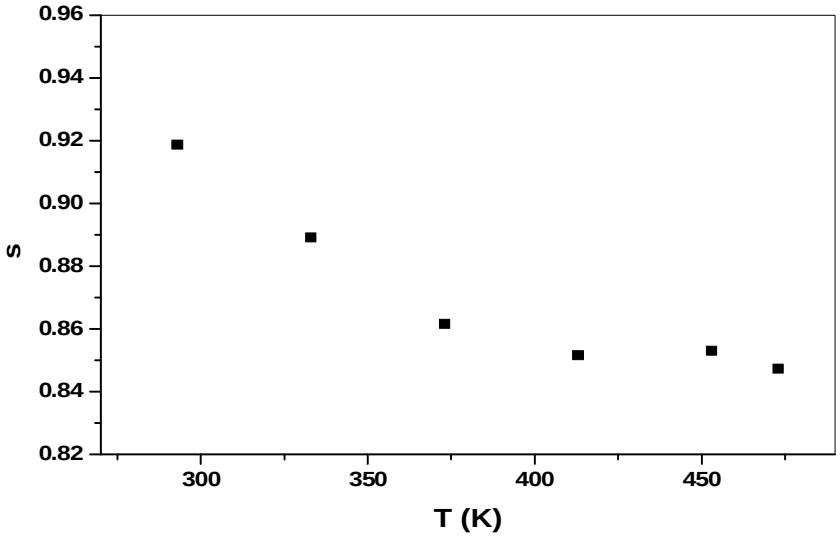

Fig.(3): Temperature dependence of frequency exponent s

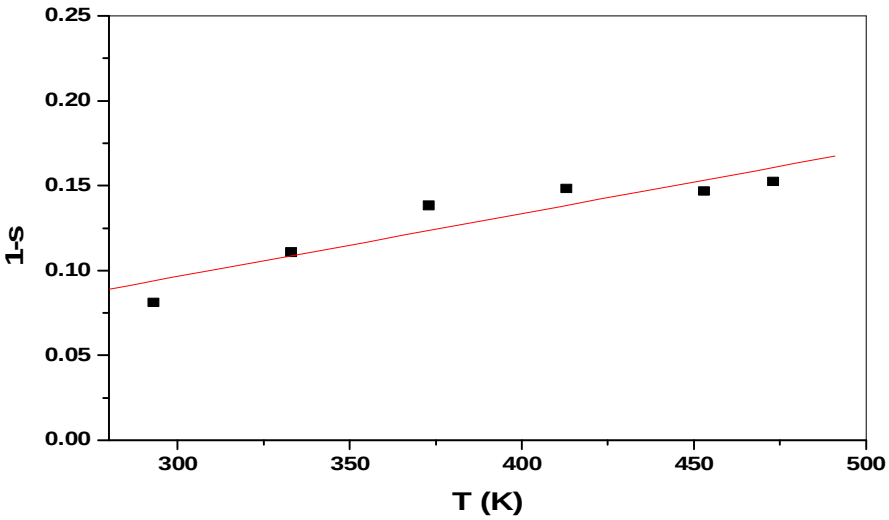

Fig.(4): Plot of 1-S against temperature.

The temperature dependence of the ac conductivity at different constant frequencies for $TlInSe_2$ is represented in Fig. (5). An Arrhenius type behavior, $\sigma_{ac} = \sigma_o \exp\left(\frac{\Delta E_{ac}}{kT}\right)$ is shown. Where σ_o is the pre-exponential factor and ΔE_{ac} is the ac conductivity activation energy. The ac conductivity increases with increasing temperature. This suggested that the ac conductivity is thermally activated process from different localized states in the gap or its tails [21,31]. The activation energy is calculated from the slopes of the linear fit of the straight

lines in Fig. (5) for $TlInSe_2$ and listed in Table1. The values of ΔE_{ac} decrease with increasing frequency. This behavior is related due to that, the increase of the applied field frequency enhances the electronic jumps between the localized states, consequently the activation energy decreases with increasing frequency [31,32].

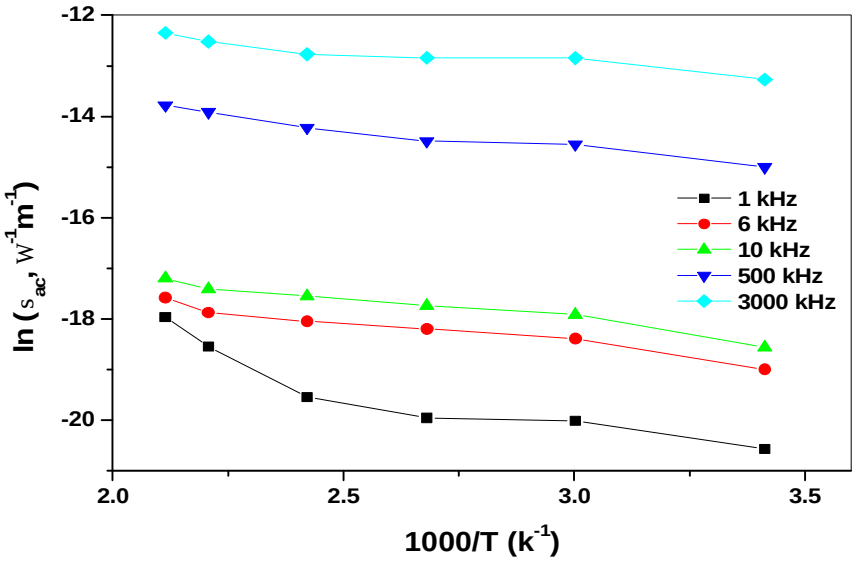

Fig.(5): Temperature dependence of σ_{ac} of $TlInSe_2$ at different frequencies.

3.2. Frequency and Temperature dependence of dielectric constant and dielectric loss

The dielectric constant, ε_1, can be calculated from the equation: $\varepsilon_1 = \frac{dC}{A\varepsilon_0}$, where C is the sample capacitance and ε_0 is the permittivity of free space. While, the dielectric loss, ε_2, was calculated from the equation: $\varepsilon_2 = \varepsilon_1 \tan\delta$.

Figures (6 and 7) presented the variation of dielectric constant (ε_1) and dielectric loss (ε_2) values with frequency at different constant temperatures for $TlInSe_2$. It is seen that both the dielectric constant and dielectric loss values decrease with increasing frequency. Such behavior of ε_1 and ε_2 is reported for $TlInS_2$ and $TlInS_2$:Cu single crystals [32,33]. Fig. (6) shows that as the temperature increases, the values of dielectric constant increases. The increase of ε_1 can be attributed to the fact that the dipoles in polar materials cannot orient themselves at low temperatures. Then when the temperature is increased the orientation of the dipoles is facilitated and thus increases the values of the orientational polarization, which in turn increases ε_1 [34]. Also, it is clear from

the figure that ε_1 decreases with increasing frequency. This can be attributed to the contribution of many components of polarization; electronic, ionic, dipolar or orientation and space charge. Electronic polarization arises from displacement of valence electrons relative to the positive nucleus. The ionic polarization occurs due to the displacement of negative and positive ions with respect to each other. Dipolar polarization occurs as a result of the presence of molecules with permanent electrical dipole moments that can change orientation into the direction of the applied electric field. Space charge polarization occurs due to impedance mobile charge carriers by interfaces. The total polarization of the dielectric material is the sum of these four polarizations [35], which is related to the dielectric constant ε_1 . In the present study, ionic polarization does play a significant role in the total polarization where the degree of covalency in $TlInSe_2$ films is estimated using Pauling equation [36]:

The portion of covalent character $= 100\%(-0.25(\xi_A - \xi_B)^2)$ (4)

where ξ_A and ξ_B are the electro negativity of atoms A and B, respectively. The values of covalent character are calculated using equation (4) and are listed in Table 2, which confirms that the bonding is predominantly covalent.

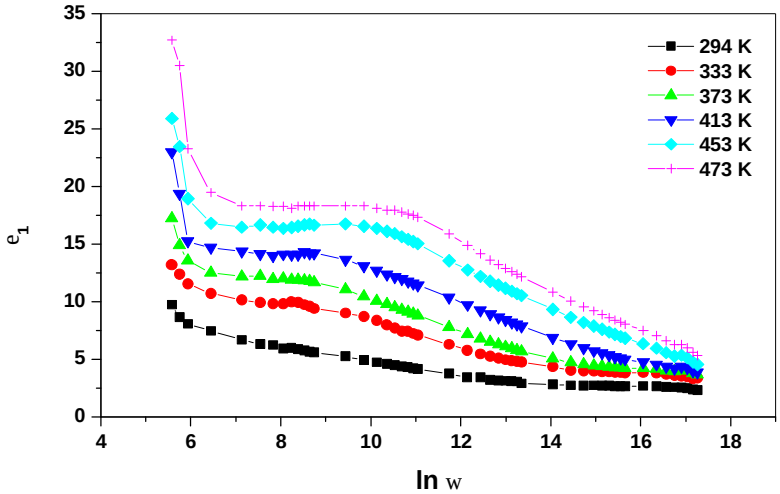

Fig. (6): Frequency dependence of ε_1 of $TlInSe_2$ at different Temperatures.

The increase of ε_1 with frequency is due the decrease of the orientation polarization, since it takes longer time than other types of polarization and the dipoles cannot be able to rotate sufficiently rapidly, so that their oscillations lag behind those of the field. As the frequency is further increased, the dipole will be completely unable to follow the field and the orientation polarization stopped; so ε_1 decreases approaching a constant value at high frequencies due to the space charge polarization only.

Figure (7) shows that the dielectric loss ε_2 increases with increasing temperature while, decreases with increasing frequency. The increase of ε_2 with temperature can be explained by Stevels [37,38] who divided the relaxation phenomena into three parts, conduction loss, dipole loss and vibrational loss. At low temperatures, the conduction loss has a minimum value science it is proportional to (σ/ω). As the temperature increases, σ increases and so the conduction loss increases. This increases the value of ε_2 with increasing temperature. Also, it is clear from Fig. (7) that ε_2 decreases with increasing frequency. The decrease of ε_2 with the increase in frequency can be attributed to the fact that the value ε_2, at low frequencies, is due to the migration of ions in the material. At moderate frequencies ε_2 is due to the contribution of ions jumps, conduction loss of ions migration, and ions polarization loss. At high frequency, ion vibrations may be the only source of dielectric loss and so ε_2 has the minimum value.

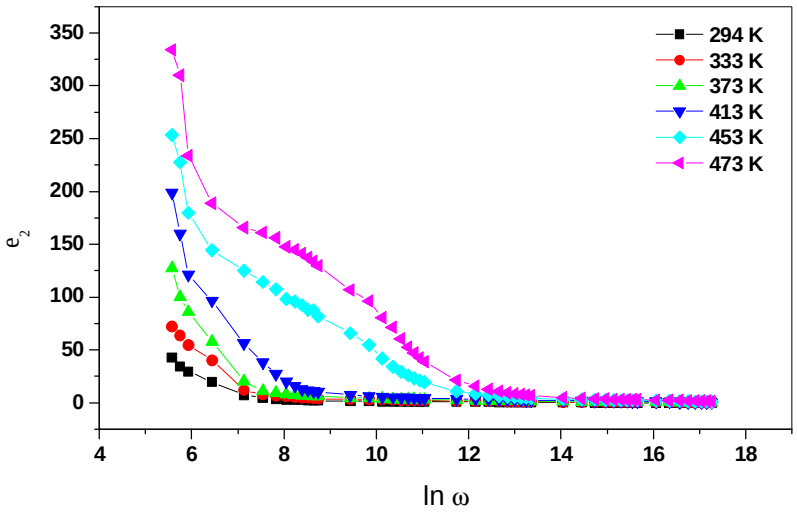

Fig. (7): Frequency dependence of ε_2 of $TlInSe_2$ at different Temperatures.

The absence of a well-defined ε_2 (ω) peak suggests that information about the relaxation mechanism can be obtained from the electric modulus representation as proposed by Moynihan, Boese and Laberage [39,40]. The dielectric modulus representation, which is defined as the reciprocal of the dielectric permittivity [41,42]:

$$M^*(\omega) = \frac{1}{\varepsilon^*(\omega)} = M'(\omega) + M''(\omega) \qquad (5)$$

where M' and M'' are the real and imaginary parts of dielectric modulus, respectively.
They defined as

$$M'(\omega) = \frac{\varepsilon_1}{[(\varepsilon_1)^2+(\varepsilon_2)^2]} \quad (6)$$

$$M''(\omega) = \frac{\varepsilon_2}{[(\varepsilon_1)^2+(\varepsilon_2)^2]} \quad (7)$$

Figures (8 and 9) show the real and imaginary parts of the electric modulus, $M'(\omega)$ and $M''(\omega)$ as a function of frequency for bulk $TlInSe_2$ at different constant temperatures. It is clear that $M'(\omega)$ increased with increasing frequency and approached zero at low frequencies. Such behavior confirmed the presence of an appreciable electrode and/or ionic polarization in the studied temperature ranges [43]. From Fig. (9), double peaks were observed in the patterns of $M''(\omega)$ for some of temperatures. These peaks were shifted toward higher frequencies with increasing temperature. The frequency region below the maximum value of M'' determines the range in which charge carriers are mobile over long distances. For frequencies above maximum value, the carriers seem to be confined to potential well, thus becoming mobile over a short distance [44].

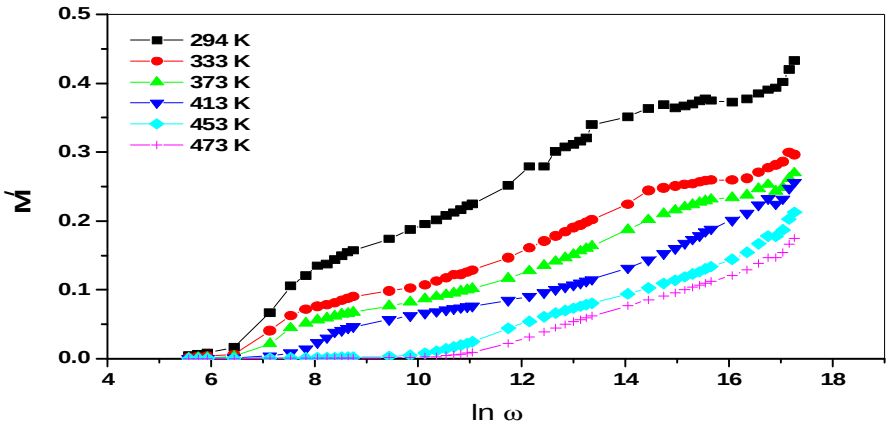

Fig. (8): Frequency dependence of $M^{/}$ of $TlInSe_2$ at different Temperatures.

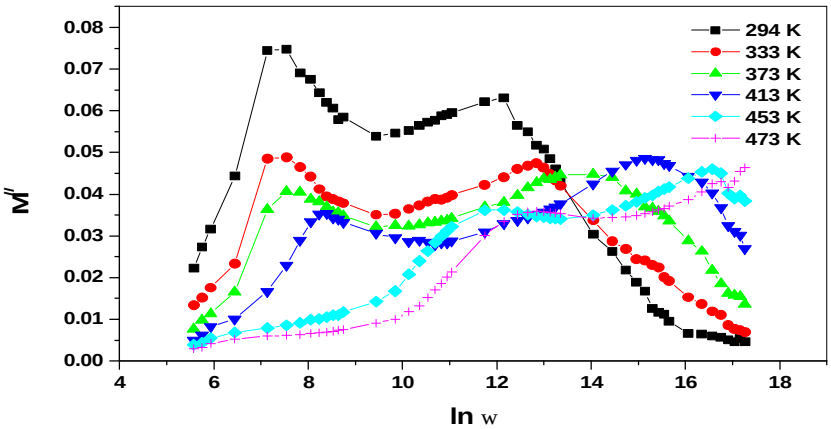

Fig. (9): Frequency dependence of $M^{//}$ of $TlInSe_2$ at different Temperatures.

The maximum peak of $M''(\omega)$ curves corresponds to the relaxation frequency ω_p such as: $\tau = 1/\omega_p$. The temperature dependence ofω_p, Fig.10, represented by the Arrhenius equation:

$$\omega_p = \omega_o \exp\left(-\frac{\Delta E_p}{kT}\right) \quad (8)$$

where ω_o is the pre-exponential factor and ΔE_p is the activation energy for the electrical relaxation processes. The value of ΔE_p extracted from the slope of the plot in Fig. (10) is found to be 0.36 eV.

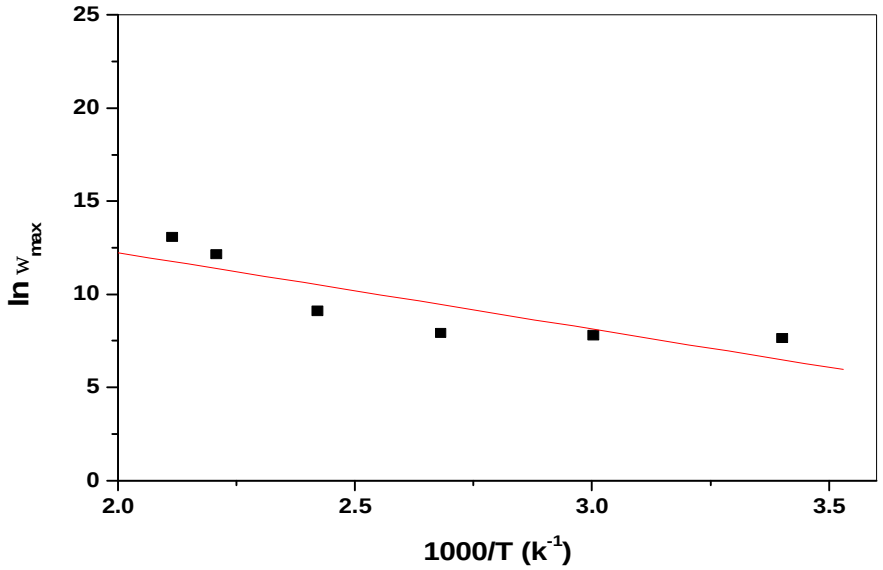

Fig. (10): The dependence of Ln ω_p versus 1000/T.

4. Conclusions

X-ray diffraction analysis showed that the powder of $TlInSe_2$ is tetragonal crystal structure. AC conductivity varies with ω^s. The temperature dependence of the exponent s supports the correlated barrier hopping model as the predominant mechanism for ac conduction. The temperature dependence of ac conductivity showes a linear increase with increasing temperature. Both dielectric constant and dielectric loss of bulk $TlInSe_2$ decreased with increasing frequency over the investigated frequency range. The real part of electric modulus increased with increasing frequency and approached zero at low frequencies. The patterns of the imaginary part of electric modulus showed double peaks for some of temperatures. The activation energy of relaxation processes was found to be 0.36 eV.

References

1. 1.M. Isik, N.M. Gasanly, H. Ozkan, *Acta Phys. Pol*. **A115**, 732 (2009).
2. K.A.Yee, A. Albright, *J. Am. Chem. Soc*., **113**, 6474 (1991).
3. S. Johnsen, Z. Liu, J.A. Peters, J. Song, S.C. Peter, C.D. Malliakas, N. KiCho, H. Jin, A.J. Freeman, B.W. Wessels, M.G. Kanatzidis, *Chem. Mater*., **23**, 3120 (2011).
4. A.A. Al-Ghamdi, A.T. Nagat, F.S. Bahabri, R.H. AlOrainy, S.E. AlGarni, *Appl. Surf. Sci*., **257**, 3205 (2011).
5. K. Mimura, K. Wakita, M. Arita, N. Mamedov, G. Orudzhev, Y. Taguchi, K. Ichikawa, H. Namatame, M. Taniguchi, *J. Electron Spectrosc. Relat. Ph*., **156**, 379 (2007).
6. K. Mimura,T. Ishizu, K. Yamamoto, J. Takasu, Y. Yonehira, K. Wakita, N. Mamedov, Y. Taguchi, K. Ichikawa, K. Yan, E. Ikenaga, K. Kobayashi, *Phys. Status Solidi*, C **6**, 993 (2009).
7. R. Sardarly, O. Samedov, A. Abdullayev, F. Salmanov, A. Urbanovic, F. Garet‹ J. Coutaz, Jpn. *J. Appl. Phys*., **50**, 05FC09 (2011).
8. I. V. Alekseev, *Semi*., **32**, 526 (1998).
9. I. V. Alekseev, *Instrum. Exp. Technol*., **51**, 331 (2008).
10. A.F. Qasrawi, N.M. Gasanly, *Mater. Sci. Semi. Pross*., **14**, 175 (2011).
11. K.R. Allakhverdiev, *Solid State Comm*., **111**, 253 (1999).
12. S.O¨ Zdemir, R.A.S ¨ Uleymanov, K.R. Allakhverdiev, F.A. Mikailov, E. Civan, *Solid State Comm*., **96**, 821 (1995).
13. N. Mamedov, K. Wakita, A. Ashida, T. Matsui, K. Morii, *Thin Solid Films*, **499**, 275 (2006).
14. A.F. Qasrawi, N.M. Gasanly, *Mater. Chem. Phys*., **14**, 63 (2013).

15. M. Hanias, A. Anagnastopoulos, K. Kambas, *J. Spyridelis, Physica*, B **160**, 154 (1989).
16. A.F. Qasrawi, N.M. Gasanly, *Mater. Res. Bull*., **46**, 1227 (2011).
17. Yu.M. Azhniuk, A.V. Gomonnai, V.M. Rubish, M.Yu. Rigan, A.M. Solomon, O.O. Gomonnai, O.G. Guranich, I. Petryshynets, D.R.T. Zahn, *J. Phys. Chem. Solids*, **74**, 1452 (2013).
18. G. Orudzhev, V. Jafarova, S. Schorr, K. Mimura, K. Wakita, Y.G. Shim, N. Mamedov, F. Hashimzade, *J. Appl. Phys*., **47**, 8193 (2008).
19. Joint Comm. On Powder Diffraction Standard (JCPDS), Amer. Soc. For Testing and Materials (ASTM), 72 (1998).
20. S.R. Elliott, *Physics of Amorphous Materials*, Wiley, New York, (1983).
21. M.M. El-Nahass, A.M. Farid, K.F. Abd El-Rahman, H.A.M. Ali, *Physica* B **403**, 2331 (2008).

22. N.F. Mott, E.A. Davis, *Electronic Processes in Non-Crystalline Materials*, Clarendon Press, Oxford, (1979).
23. S.R. Elliott, *Adv. Phys*., **36**, 135 (1987).
24. A.K. Jonscher, *Nature*, 267, 673 (1977).
25. A. Ganjoo, A. Yoshida, K. Shimakawa, *J. Non-Cryst. Solids*, **198**, 313 (1998).
26. M. Pollak, T. H. Geballe, *Phys. Rev*., B **122**, 1742 (1961).
27. S.R. Elliott, *Philos. Mag*. B **37**, 553 (1978).
28. K. Shimakawa, *Phil. Mag*., **46**, 123 (1982).
29. M. S. Hossain, R. Islam, K. A. Khan, *Chalcogenide Letters*, **5** (1), 1 (2008).
30. G.E. Pike, *Phys. Rev*., B **6**, 1572 (1972).
31. A.A.A. Darwish, M.M. El-Nahass, A.E. Bekheet, *J. Alloys Compd*., **586**, 142 (2014).
32. M.M. El-Nahass, H.A.M. Ali, E.F.M. El-Zaidia, *Physica* B, **431**, 52 (2013).
33. M.M. El-Nahass, S.B. Youssef, H.A.M. Ali, A. Hassan, *Eurp. Phys. J. Appl. Phys*., **55**, 10101 (2011).
34. V. Gupta, K.K. Bamzai, P.N. Kotru, B.M. Wanklyn, *Mater. Sci*. Eng. B, **130**, 163 (2006).
35. M. Barsoum, *Fundamental of Cerimcs*, New York; McGraw-Hill, 543 (1977).
36. L. Paulling, *The Nature of the Chemical Bond*, New York: Cornell University, (1960).
37. J.M. Stevels, *The Electrical Properties of Glasses*, Handbuch der Pysik, 350 (1975).
38. S.S. Fouad, A.E. Bekheet, A.M. Farid, *Physica*, B **322**, 163 (2002).
39. C.T. Moynihan, R. Bose, F. Laberage, *Phys. Chem. Glass*. 14, 22 (1973).
40. C.T. Moynihan, *Solid State Ionics*, **105**, 175 (1998).
41. A. Moguš-Milanković, B. Šantić,, D.E. Day, C.S. Ray, *J. Non-Cryst. Solids* **283**, 119 (2001).
42. A. Dutta, C. Bharti, T.P. Sinha, *Ind. J. Engineer. Mater. Sci*., **15**, 181 (2008).
43. M.P. Dasari, K. S. Rao, P. M. Krishna, G.G. Krishna, *Acta Phys. Pol*., A **119**, 387 (2011).
44. A. Moguš-Milanković, A. Šantić, V. Liĉina, D.E. Day, *J. Non-Crryst. Solids*, **351**, 3235 (2005).